Mineralogical Magazine, November 2014, Vol. 78(6), pp. 1391–1397

OPEN ACCESS

The effect of heating on the morphology of crystalline neodymium hydroxycarbonate, $NdCO_3OH$

BEATRIZ VALLINA[1,*], JUAN DIEGO RODRIGUEZ-BLANCO[1,2], JESUS A. BLANCO[3] AND LIANE G. BENNING[1,4,*]

[1] School of Earth and Environment, University of Leeds, Leeds LS2 9JT, UK
[2] Nano-Science Center, Department of Chemistry, University of Copenhagen H.C Oersted Institute, C Bygn, Universitetsparken 5, DK 2100 Copenhagen, Denmark
[3] Departamento de Física, Universidad de Oviedo, Oviedo, E-33007, Spain
[4] GFZ German Research Centre for Geosciences, Helmholz Centre Potsdam, Telegrafenberg, 14473 Potsdam, Germany

[*Received 4 May 2014; Accepted 3 October 2014; Associate Editor: T. Rinder*]

ABSTRACT

The crystallization of hexagonal $NdCO_3OH$ through hydrothermal synthesis carried out at slow (reaching the desired temperature within 100 min) and quick (50 min) rates of heating but at variable temperatures (165−220ºC) are reported here. The formation of $NdCO_3OH$ occurs *via* the crystallization of an amorphous precursor. Both the precursor and the crystalline $NdCO_3OH$ were characterized by X-ray diffraction, infrared spectroscopy and high-resolution electron microscopy. The mechanism of crystallization is very dependent on the experimental conditions (rate of heating and temperature treatment). With increasing temperature, the habit of $NdCO_3OH$ crystals changes progressively to more complex spherulitic or dendritic morphologies. The development of these crystal morphologies is suggested here to be controlled by the level at which supersaturation was reached in the aqueous solution during the breakdown of the amorphous precursor. At the highest temperature (220ºC) and during rapid heating (50 min) the amorphous precursor breaks down rapidly and the fast supersaturation promotes spherulitic growth. At the lowest temperature (165ºC) and slow heating (100 min), however, the supersaturation levels are approached more slowly than required for spherulitic growth, and thus more regular, previously unseen, triangular pyramidal shapes form.

KEYWORDS: rare earths, neodymium, carbonate, crystallization, spherulitic growth, hydroxylbastnäsite.

Introduction

THE formation of carbonate minerals plays a crucial role in controlling the global carbon cycle (Mackenzie and Andersson, 2013). Carbonate deposits have formed ubiquitously throughout the geological record and these are now often used for various industrial applications. Among the carbonate systems of interest, rare earth carbonates are of prime importance as they are the main source for the much sought after rare earth elements (*REE*) in the modern industrial world. Among *REE* carbonates, specifically hydroxycarbonates, $REECO_3(OH)$, constitute the most important group of *REE* compounds that are highly valued for a plethora of industrial processes such as automotive, ceramics, oil, metallurgy, high-performance luminescent devices, magnets, etc. (Adachi and Imanaka, 1998; Castor and Hedrick, 2006). Two

* E-mail: B.Vallina-Antuna@leeds.ac.uk; l.g.benning@leeds.ac.uk
DOI: 10.1180/minmag.2014.078.6.05

This paper is published as part of a special issue in *Mineralogical Magazine*, Vol. **78(6)**, 2014 entitled 'Mineral–fluid interactions: scaling, surface reactivity and natural systems'.

REECO_3(OH) polymorphs (orthorhombic and hexagonal) have been described, with the hexagonal polymorph of the neodymium hydroxycarbonate occurring in *REE* deposits as the mineral hydroxylbastnäsite (e.g. Bayan Obo deposit, China; Zhongxin *et al*., 1992). Nd-hydroxylbastnäsite [$NdCO_3(OH)$] is believed to form through hydrothermal reactions with sedimentary carbonate rocks, yet a mechanism for this process is still unknown (Miyawaki and Nakai, 1996). The interest in understanding the formation pathways of Nd-hydroxylbastnäsite is also linked to its role in optical (e.g. lasers) and electronic (e.g. neodymium-iron-boron permanent magnets) applications (Chakhmouradian and Wall, 2012). Most previous studies addressed the $NdCO_3(OH)$ structure (e.g. Christensen 1973; Michiba *et al*., 2011; Tahara *et al*. 2007) or its decomposition behaviour (Hinode *et al*., 1990) under hydrothermal conditions. Those studies, revealed that various synthesis conditions lead to hexagonal $NdCO_3(OH)$ crystals with different morphologies (e.g. hexagonal prisms, dendrites or rodlike crystals; Michiba *et al*., 2011; Shang *et al*., 2009; Gai *et al*., 2014). Such morphologies play a key role in the physicochemical properties of many materials involved in technological advances in magnetic, electronic and optoelectronic devices (Gai *et al*., 2014; Li *et al*., 2013; Shang *et al*., 2009; Vallina *et al*., 2014). However, the factors that control the formation conditions or the possible morphologies of hexagonal $NdCO_3(OH)$ are not well understood.

To address this, the present authors carried out hydrothermal crystallization experiments with the goal of producing hexagonal $NdCO_3(OH)$ from a poorly ordered precursor. This was done at different rates of heating (slow and fast) and different temperatures (165−200ºC) to evaluate the effects of these two parameters on the crystallinity and morphology of the hexagonal $NdCO_3(OH)$ product. The morphologies of the resulting $NdCO_3(OH)$ are proposed here to be a consequence of varying crystallization mechanisms that in turn are controlled by the degree of supersaturation after the breakdown of a poorly ordered Nd-carbonate precursor.

Experimental

Neodymium carbonates were synthesized by adding a 50 mM solution of $NdCl_3{\cdot}H_2O$ (Alfa Aesar, 99% purity) to a 50 mM Na_2CO_3 solution (Fisher Scientific, 99.9% purity) at room temperature (RT, 21ºC). Immediately after mixing, a pink gel-like precipitate formed. Aliquots of this material were treated using four different hydrothermal treatment approaches. The hydrothermal crystallization reactions were carried out in Teflon-lined stainless steel (40 ml; Parr®) reactors in ovens at temperatures between 25 and 220ºC and at saturated water-vapour pressures and all were reacted for 1 week. Two aliquots of the pink gel-like precursor (referred to hereafter as batches A and B) were aged in their native solution at 165 and 220ºC. This was achieved by half filling a reactor at RT with pink gel, inserting into a preheated oven at the desired temperature and shaking the reactor manually every 20 min. Tests have shown that the desired temperature inside the reactors was reached within ~100 min (at 165ºC) and ~50 min (at 220ºC). The other two aliquots (batches C and D) were aged in their native solution at 220ºC but using a different heating protocol, where the temperature was ramped to 220ºC at a constant rate of 10ºC/min. Batch D was ramped from 25 to 220ºC, while batch C was inserted into an oven that was already preheated to 100ºC and subsequently ramped to 220ºC. Although the temperature ramps reached the desired temperature within 20 min, the temperature of the suspension inside the reactors in these two batches was reached more slowly. A schematic summary of all four experiments is shown in Fig. 1.

To characterize the initial pink gel and the final reaction products (after quenching to room temperature) sample slurries were vacuum filtered through 0.2 μm polycarbonate membranes, washed with water and isopropanol following Rodriguez-Blanco *et al*. (2008) and dried at RT. The resulting solids were characterized by powder X-ray diffraction (XRD; Bruker D8 diffractometer; Cu$K\alpha_1$; 10−75º2θ; 0.005º/step and 0.1 s/step), Fourier transform infrared (FTIR) spectroscopy (A2 Technologies MicroLab spectrometer; spectra collected between 650 and 4000 cm^{-1}; 4 cm^{-1} resolution and by co-adding 1024 scans). Furthermore, all solids were imaged and analysed using a field emission gun scanning electron microscope (FEG-SEM, LEO 1530 Gemini, operated at 3 kV and with an in-lens detector and a FEG-transmission electron microscope, FEG-TEM; FEI CM200; operated at 197 kV).

The saturation index (SI) with respect to the crystalline solids was calculated using the computer code *PHREEQC* (Parkhurst, 1995, using the LLNL database) and is defined as the

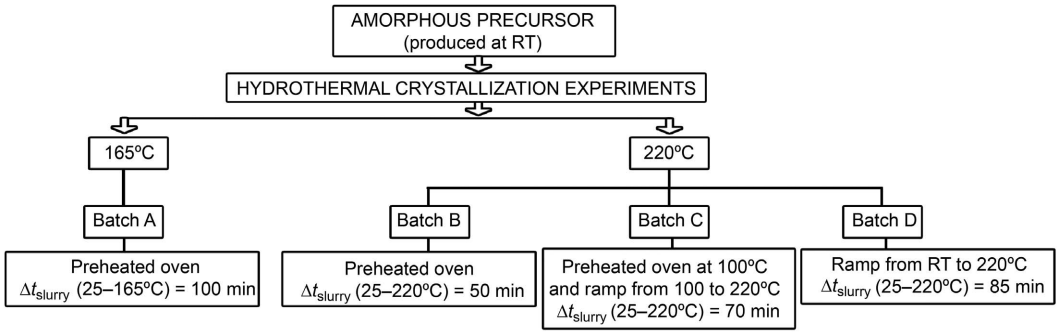

FIG. 1. Summary of the experiments. Δt_{slurry} designates the time taken for the amorphous precursor to reach the desired temperature under the stated heating regime.

ratio between the ionic activity product (*IAP*) of the dissolved ions and the solubility product of the solid phase (K_{sp}):

$$SI = \log IAP/K_{sp} \quad (1)$$

Taking equation 1 into account, the saturation index (SI) is positive when the solution is supersatured with respect to the solid phase, and negative when it is undersaturated.

Results and discussion

The FEG-TEM images of the initial pink gel-like phase revealed roughly spherical nanoparticles with diameters of between 10 and 20 nm (Fig. 2*a*) and with few to no lattice fringes visible. Powder XRD patterns of the gel contained only three broad humps centred at ~20, 30 and 45º2θ indicating that the gel was poorly crystalline (Fig. 2*b*). The FTIR spectra (Fig. 2*c*) confirmed the carbonate (bands between 1450 and 680 cm^{-1}), highly hydrated (broad band at ~ 3000 cm^{-1}), and poorly ordered nature of the Nd-carbonate gel (lack of peak at 725 cm^{-1}; for a similar pattern for a Dy-carbonate gel see Vallina *et al*., 2013).

Upon hydrothermal treatment, this amorphous phase transformed to a crystalline material the XRD pattern of which matched in all cases that of hexagonal neodymium hydroxycarbonate, $NdCO_3OH$ (a = 12.3579(11) Å and c = 9.9025(9) Å; Fig. 2*d*). The FEG-SEM images of the final products revealed different morphologies, however, depending on the heating and temperature. The solids at the end of the reaction in batch A (165ºC, normal heating, no controlled temperature ramp) exhibited regular, triangular pyramidal shapes with large individual crystals ~8 μm in diameter (Fig. 3*a*,*b*), while under the same heating regime but at 220ºC in batch B (normal heating, no controlled temperature ramp), cauliflower-like aggregates (up to 25 μm in diameter) were observed. These cauliflower-like aggregates had very complex micro-textures and were made up of small crystal subunits that were <500 nm in size (Fig. 3*c*,*d*). When the initial amorphous precursor gel was heated from 100 to 220ºC through a 10ºC/min temperature ramp (batch C), the resulting morphologies were different again. Spine-shaped aggregates between 10 and 25 μm in size consisting of subunits 1−5 μm long were formed (Fig. 3*e*,*f*). Finally, when the suspension was heated from RT to 220ºC with a 10ºC/min ramp (batch D) the end product consisted of long fishbone-shaped morphologies (up to 25 μm long) but again consisting of subunits with crystals of <1 μm (Fig. 3*g*,*h*).

The data above show clearly that in the 220ºC experiments, even small differences in heating procedures led to significantly different morphologies for the resulting hexagonal $NdCO_3(OH)$ crystals. In addition, the present study is the first to report triangular pyramids and spine shapes for the highly crystalline hexagonal $NdCO_3OH$. In contrast the fishbone and cauliflower morphologies (although somewhat different in terms of dimensions) are similar to those reported by Shang *et al*. (2009) who synthesized fishbone or cauliflower $NdCO_3OH$ much more quickly using an hydrothermal synthesis at 220ºC over a period of 6 h. Such shape differences are important, as idiomorphic, well developed crystals of hexagonal $NdCO_3OH$ are of interest for use in modern optical technologies (Li *et al*., 2013).

Our experiments show that $NdCO_3OH$ develops the more regular morphologies at

lower temperatures and the slowest rate of heating (165ºC, 100 min; batch A). At the highest temperature (220ºC) and with a higher rate of heating (85−50 min; batches B−D) the resulting $NdCO_3OH$ morphologies were dendritic and similar to those of Shang *et al.* (2009) or similar to spherulitic crystal aggregates reported for other carbonate systems (e.g. calcium carbonates – Sand *et al*., 2012; Bots *et al*., 2012 and references therein; calcium phosphate – Teshima *et al*., 2009; and lanthanum carbonates – Sadhu *et al*., 2014). Spherulites, as observed in our experiments (Fig 3*c*,*d* and *e*,*f*), are most often interpreted as a result of continuous nucleation of new particles with random orientations (Shtukenburg *et al*., 2012). Such processes also require high levels of supersaturation throughout the whole crystallization reaction (e.g. Beck and Andreassen, 2010; Bots *et al*., 2012). In our experiments, supersaturation levels at 220ºC could not be calculated because no solubility data for crystalline $NdCO_3OH$ or the amorphous precursor exists in the literature. However, solubility data for the crystalline neodymium lanthanite ($Nd_2CO_3{\cdot}8H_2O$) is only available at 25ºC (Essington and Mattigod, 1985) and no solubility data for hexagonal Nd-hydroxylbastnäsite are available. The solubility data for $Nd_2CO_3{\cdot}8H_2O$ are used here as a proxy for hexagonal Nd-hydroxylbastnäsite. This analogy is justifiable because of the processes observed here compared with those in other carbonate systems (e.g. $CaCO_3$) where equivalent reactions prevail (Rodriguez-Blanco *et al*., 2011; Bots *et al*., 2012). The saturation index, SI (equation 1), for neodymium lanthanite ($Nd_2CO_3{\cdot}8H_2O$) at 25ºC is $SI_{Nd\text{-}lanth}$ = 11.01. As with many other carbonates (Plummer and Busenberg, 1982) it is expected that the solubility of $Nd_2CO_3{\cdot}8H_2O$ will decrease with temperature and thus by analogy with other systems, leads us to assume that the SI of the present crystalline $NdCO_3OH$ will also increase with temperature and thus, at 220ºC, the likely $SI_{Nd\text{-}hyrbast}$ will be >11.01. Such high SI

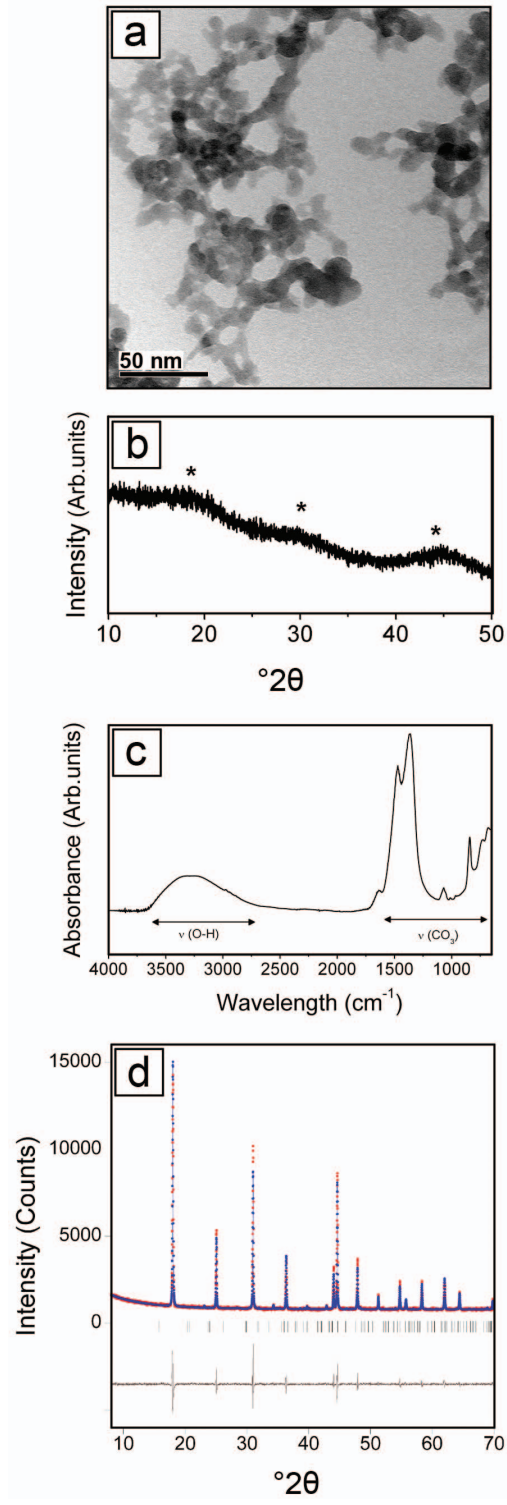

FIG. 2. (*a*) TEM image of the initial precursor showing spherical nanoparticles with diameters of between 10 and 20 nm; (*b*) XRD pattern of the gel-like precursor showing its amorphous character; (*c*) FTIR profile of the precursor showing bands corresponding to water and carbonate vibrations; and (*d*) pattern-matching refinement of the XRD pattern of the final end product indexed as hexagonal $NdCO_3(OH)$.

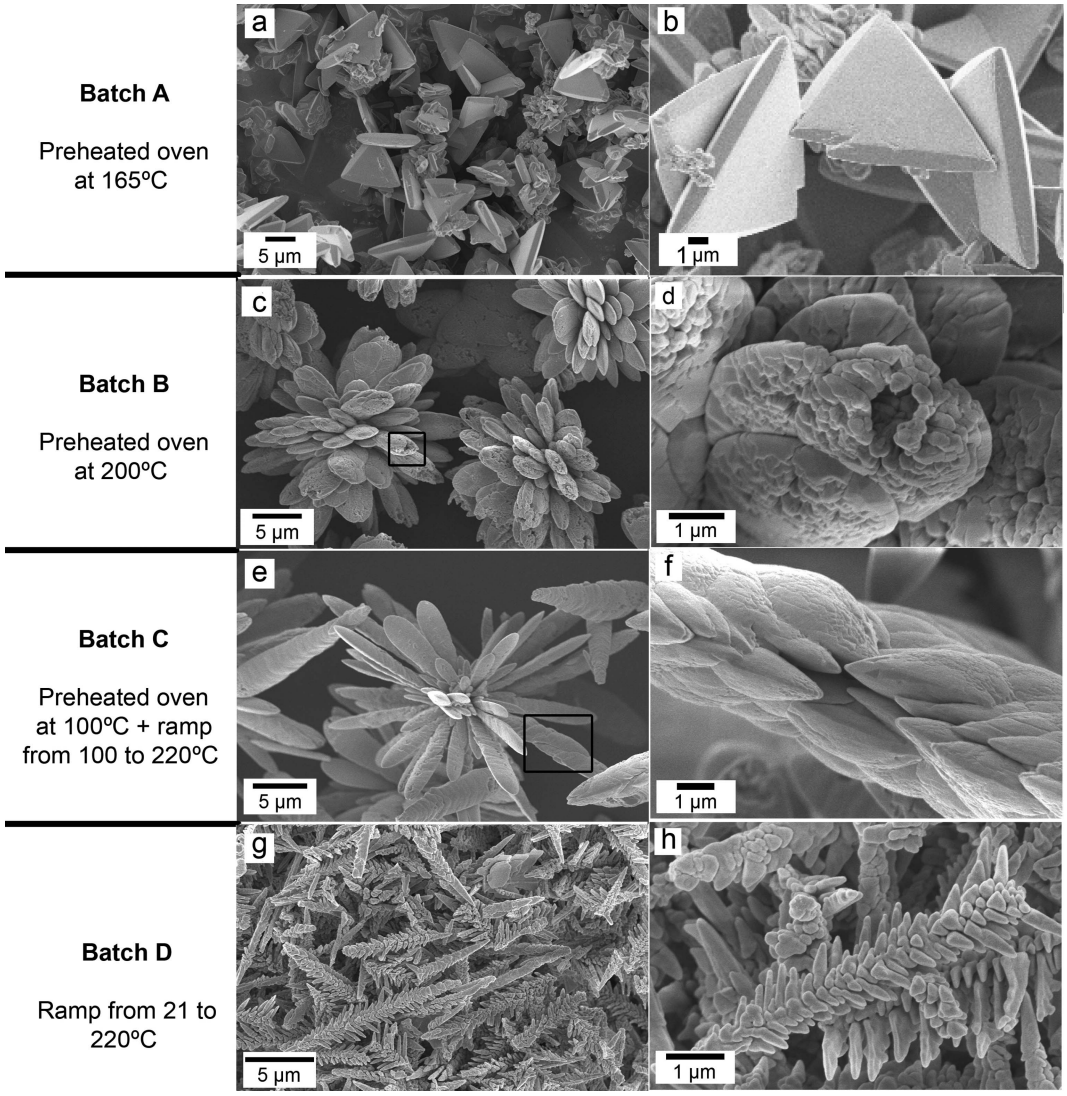

FIG. 3. FEG-SEM images of $NdCO_3(OH)$ produced *via* the four different hydrothermal treatments. The habits are changing as a function of the experimental conditions. (*a*,*b*) Triangular pyramid shapes obtained from batch A; (*c*,*d*) cauliflower-type morphologies obtained from batch B; (*e*,*f*) spine-shaped aggregates developed with batch C; (*g*,*h*) fishbone (dendritic) morphologies obtained with a heating ramp from 21 to 220ºC (Batch D).

values are typical for systems where spherulitic growth prevails (Shtukenberg *et al*., 2012). Such growth often leads to cauliflower-like or dendritic shapes during the breakdown and crystallization of the amorphous precursor (e.g. Sand *et al*., 2012; Bots *et al*., 2012).

Equivalent, poorly ordered, hydrated carbonate precursors (Rodriguez-Blanco *et al*., 2011, 2014), are known to break down through a combination of spherulitic growth, dissolution/re-precipitation and dehydration (e.g. Radha *et al*., 2010; Bots *et al*., 2012; Saharay, 2013) and such breakdown reactions are often also highly temperature-dependent (e.g. for Dy-carbonate; Vallina *et al*., 2013). Current data on the crystallization of hexagonal $NdCO_3OH$ also imply that as well as the reaction temperature, a second important parameter is the rate of heating. Higher heating

rates will result in a quicker approach to the superaturation level needed to initiate the precursor breakdown. The faster the desired temperature is reached the more non-equilibrium, dendritic or spherulitic crystals that form. This explains the absence of spherulitic morphologies in the experiment at 165ºC, where the temperature was low and the time taken to reach this low temperature (100 min) was greater than in the other experiments. Thus, conditions were not suitable for inducing a quick breakdown of the amorphous precursor and in this experiment the supersaturation with respect to hexagonal $NdCO_3OH$ was approached more slowly and thus the growth of the $NdCO_3OH$ crystals was slower, leading to larger, more isometric crystals.

Conclusions

A reproducible hydrothermal synthesis method to control the morphologies of hexagonal $NdCO_3OH$ has been demonstrated. The development of crystals of variable size and of simple or complex morphologies of $NdCO_3OH$ (i.e. small surface area and low-complexity triangular pyramids – batch A *vs*. large surface area and high-complexity, fishbone-shaped crystals – batch D) depends on the synthesis conditions. The lowest temperature and slowest rate of heating led to regular but new forms. These change progressively at higher temperature (220ºC) and with increasing heating speed leading to the development of spherulitic and other more complex shapes. We interpret the origin of the different morphologies to be a consequence of the increasing level at which supersaturation in solution was approached prior to the onset of crystallization (i.e. breakdown of the amorphous precursor phase). Higher temperatures and faster heating promote rapid crystallization, favouring spherulitic growth.

Acknowledgements

This research was supported by the Marie Curie EU-FP7 CO2-REACT Research and Training Network under contract RG.EVEA.101025-004. The authors thank their colleagues in the Cohen Laboratories at the School of Earth and Environment and Andrew Brown from the Leeds Electron Microscopy and Spectroscopy Centre (LEMAS) at the Faculty of Engineering (Leeds, UK) and the Spanish Ministry of Economy and Competitiveness (MICINN-12-MAT2011-27573-C04-02) for help during the study. They also thank the Associate Editor and the three reviewers whose insightful comments helped improve the manuscript.

References

Adachi, G.Y. and Imanaka, N. (1998) The binary rare earth oxides. *Chemical Reviews*, **98**, 1470–1514.

Beck, R. and Andreassen, J. (2010) Spherulitic growth of calcium carbonate. *Crystal Growth & Design*, **10**, 2934–2947.

Bots, P., Benning, L.G., Rodriguez-Blanco, J.D., Roncal-Herrero, T. and Shaw, S. (2012) *Crystal Growth and Design*, **12**, 3806–3814.

Castor, S.B. and Hedrick, J.B. (2006) Rare earth elements. Pp. 769–792 in: *Industrial Minerals and Rocks* (J. Elzea Kogel, N.D. Trivedi and J.M. Barker, editors). Society for Mining, Metallurgy and Exploration, Littleton, Colorado, USA.

Chakhmouradian, A.R. and Wall, F. (2012) Rare earth elements: minerals, mines, magnets (and more). *Elements*, **8**, 333–340.

Christensen, A.N. (1973) Hydrothermal preparation of rare earth hydroxy-carbonates. The crystal structure of $NdOHCO_3$. *Acta Chemical Scandinavica*, **27**, 2973–2982.

Essington, M.E. and Mattigod, S.V. (1985) Lanthanide solid phase speciation. *Solid Science Society of America Journal*, **49**, 1387–1393.

Gai, S., Li, C., Yang, P. and Lin, J. (2014) Recent progress in rare earth micro/nanocrystals: soft chemical synthesis, luminescent properties, and biomedical applications. *Chemical Reviews*, **114**, 2343–2389.

Hinode, H., Sharma, R. and Eyring, L.A. (1990) Study of the decomposition of neodymium hydroxy carbonate and neodymium carbonate hydrate. *Journal of Solid State Chemistry*, **84**, 102–117.

Li, R., Li, L., Wang, J., Li, Z., Liu, Q., Yu, J., Zhang, X., Ji, H., Zhang, M., Wei, H. and Liu, L. (2013) Influence of morphology and Yb^{3+} concentration on blue and red luminescence of uniform cube-like Y_2O_3:Yb^{3+}/Tm^{3+} particles. *Materials Chemistry and Physics*, **141**, 990–996.

Mackenzie, F.T. and Andersson, A.J. (2013) The marine carbon system and ocean acidification during Phanerozoic time. *Geochemical Perspectives*, **2**, 1–227.

Michiba, K., Tahara, T., Nakai, I., Miyawaki, R. and Matsubara, S. (2011) Crystal structure of hexagonal $RE(CO_3)OH$. *Zeitschrift für Kristallographie*, **226**, 518–530.

Miyawaki, R. and Nakai, I. (1996) Crystal chemical aspects of rare earth minerals. Pp. 21–37 in: *Rare Earth Minerals: Chemistry, Origin and Ore Deposits*

(A.P. Jones, F. Wall and C.T. Williams, editors). Chapman & Hall, London, 372 pp.

Parkhurst, D.L. (1995) User′s guide to PHREEQC – A computer program for speciation, reaction-parth, advective-transport, and inverse geochemical calculations. U.S. Geological Survey Water-Resources Investigations, Report 95-4227.

Plummer, N.L. and Busenberg, E. (1982) The solubilities of calcite, aragonite and vaterite in CO_2-H_2O solutions between 0 and 90ºC, and an evaluation of the aqueous model for the system $CaCO_3$-CO_2-H_2O. *Geochimica et Cosmochimica Acta*, **46**, 1011–1040.

Radha, A.V., Forbes, T.Z., Killian, C.E., Gilbert, P.U.P.A. and Navrotsky, A. (2010) Transformation and crystallization energetics of synthetic and biogenic amorphous calcium carbonate. *Proceedings of the National Academy of Science of the United States of America*, **107**, 16348–16443.

Rodriguez-Blanco, J.D., Shaw, S., Bots, P., Roncal-Herrero, T. and Benning, L.G. (2014) The role of Mg in the crystallization of monohydrocalcite. *Geochimica et Cosmochimica Acta*, **127**, 204–220.

Rodriguez-Blanco, J.D., Shaw, S. and Benning, L.G. (2011) The kinetics and mechanisms of amorphous calcium carbonate (ACC) crystallization to calcite, via vaterite. *Nanoscale*, **3**, 265–271.

Rodriguez-Blanco, J.D., Shaw, S. and Benning, L.G. (2008) How to make stable ACC: protocol and structural characterization. *Mineralogical Magazine*, **72**, 283–286.

Sadhu, A., Singh, S.P. and Bhattacharyya, S. (2014) Direct correlation of the morphologies of metal carbonates, oxycarbonates, and oxides synthesized by dry autoclaving to the intrinsic properties of the metals. *Crystal Growth and Design*, **14**, 4050–4067.

Saharay, M., Yazaydin, A.O. and Kirkpatrick, R.J. (2013) Dehydration-induced amorphous phases of calcium carbonate. *Journal of Physical Chemistry B*, **117**, 3328–3336.

Sand, K.K., Rodriguez-Blanco, J.D., Makovicky, E., Benning, L.G. and Stipp, S.L. (2012) Crystallization of $CaCO_3$ in water/alcohol mixtures: spherulitic growth, polymorph stabilization and morphology change. *Crystal Growth and Design*, **12**, 842–853.

Shang, X., Lu, W., Yue, B., Zhang, L., Ni, J. and Feng, Y. (2009) Synthesis of three-dimensional hierarchical dendrites of $NdOHCO_3$ via a facile hydrothermal method. *Crystal Growth and Design*, **9**, 1415–1420.

Shtukenberg, A.G., Punin, Y.O., Gunn, E. and Kahr, B. (2012) Spherulites. *Chemical Reviews*, **112**, 1805–1838.

Tahara, T., Nakai, I., Miyawaki, R. and Matsubara, S. (2007) Crystal chemistry of $RE(CO_3)OH$. *Zeitschrift für Kristallographie*, **222**, 326–334.

Teshima, K., Sakurai, M., Lee, S., Yubuta, K., Ito, S., Suzuki, T., Shishido, T., Endo, M. and Oishi, S. (2009) Morphologically controlled fibrous spherulites of an apatite precursor biocrystal. *Crystal Growth and Design*, **9**, 650–652.

Vallina, B., Rodriguez-Blanco, J.D., Brown, A.P., Blanco, J.A. and Benning, L.G. (2013) Amorphous dysprosium carbonate: characterization, stability, and crystallization pathways. *Journal of Nanoparticle Research*, **15**, 1438–1450.

Vallina, B., Rodriguez-Blanco, J.D., Brown, A.P., Blanco, J.A. and Benning, L.G. (2014) Enhanced magnetic coercivity of α-Fe_2O_3 obtained from carbonated 2-line ferrihydrite. *Journal of Nanoparticle Research*, **16**, 2322.

Zhongxin, Y., Ge, B. and Chenyu, W. (1992) Geological features and genesis of the Bayan Obo REE ore deposit, Inner Mongolia, China. *Applied Geochemistry*, **7**, 429–442.